Article

The Effect of Copolymer-Based Nanoparticle Composition (MEO$_2$MA-OEGMA) on the Release Profile of Doxorubicin *In Vitro*

Zied Ferjaoui, Eric Gaffet [ID] and Halima Alem *[ID]

Université de Lorraine—CNRS, IJL, F-54000 Nancy, France; ferjaoui1zied@gmail.com (Z.F.);
eric.gaffet@univ-lorraine.fr (E.G.)
* Correspondence: halima.alem@univ-lorraine.fr

Abstract: The release of drugs from core/shell nanoparticles (NPs) is a crucial factor in ensuring high reproducibility, stability, and quality control. It serves as the scientific basis for the development of nanocarriers. Several factors, such as composition, composition ratio, ingredient interactions, and preparation methods, influence the drug release from these carrier systems. The objective of our study was to investigate and discuss the relationship between modifications of core/shell NPs as multifunctional drug delivery systems and the properties and kinetics of drug release using an in vitro drug release model. In this paper, we prepared four core/shell NPs consisting of a superparamagnetic iron oxide NPs (Fe$_{3-\delta}$O$_4$) core encapsulated by a biocompatible thermo-responsive copolymer, poly(2-(2-methoxy) ethyl methacrylate-oligo (ethylene glycol) methacrylate) or P(MEO$_2$MAx-OEGMA$_{100-x}$) (where x and 100 − x represented the molar fractions of MEO$_2$MA and OEGMA, respectively), and loaded with doxorubicin (DOX). Colloidal behavior measurements in water and PBS as a function of temperature showed an optimization of the lower critical solution temperature (LCST) depending on the molar fractions of MEO$_2$MA and OEGMA used to form each NPs. In vitro studies of doxorubicin release as a function of temperature demonstrated a high control of release based on the LCST. A temperature of approximately 45 °C for 60 h was sufficient to release 100% of the DOX loaded in the NPs for each sample. In conclusion, external stimuli can be used to modulate the drug release behavior. Core/shell NPs hold great promise as a technique for multifunctional drug delivery systems.

Keywords: drug delivery; copolymer; LCST

1. Introduction

Cancer remains a significant global health challenge, with millions of lives affected by its devastating impact [1,2]. Conventional cancer therapies, such as chemotherapy [3], radiation, and surgery, often suffer from limitations including systemic toxicity, drug resistance, and limited selectivity towards cancer cells [4]. Over the past decades, nanotechnology has emerged as a promising field for the development of novel therapeutic approaches to overcome these challenges.

Core/shell nanoparticles (NPs), with their unique physicochemical properties and versatile surface characteristics, have gained significant attention as potential vehicles for targeted drug delivery and cancer treatment [5]. These nanoscale carriers can be engineered to encapsulate and deliver therapeutic agents specifically to tumor sites, while minimizing off-target effects on healthy tissues [6]. Moreover, their tunable properties enable controlled release of drugs, leading to enhanced efficacy and reduced side effects. Furthermore, prolonged drug release aims to improve therapeutic efficacy, reduce administration frequency, preserve drug stability, and enhance bioavailability [6]. These advantages collectively contribute to the optimization of medical treatments, resulting in more effective outcomes and improved quality of life for patients.

Core/shell NPs, particularly thermo-sensitive NPs, have attracted growing interest as promising platforms for controlled release of active pharmaceutical ingredients [7,8]. These systems are designed with a core containing the active ingredient and a temperature-sensitive shell that can modulate the release of the active ingredient in response to thermal stimuli. Several recent studies have explored the use of thermo-sensitive core/shell NPs for controlled release of active pharmaceutical ingredients. For example, in a study published by Sonal Deshpande et al. [7], core/shell NPs composed of a gold core and a poly(N-isopropylacrylamide) (PNIPAM) shell were used for controlled release of doxorubicin. Three different compositions of polymeric shells, consisting of pure pNIPAm and p(NIPAm-co-NIPMAm) with a NIPAm/N-(isopropylmethacrylamide) (NIPMAm) ratio of 1:1 (pNIPMAm50) and 1:3 (pNIPMAm75), were synthesized. The researchers found the polymer coating did not affect the heating efficiency of gold NPs by RF and enabled temperature-dependent release of doxorubicin, allowing for controlled release by adjusting the temperature. Similarly, in a study conducted by Ji Liu et al. [8], core-corona gold/poly(vinyl alcohol)-b-poly(N-vinylcaprolactam) NPs (gold@PVOH-b-PNVCL NPs) were synthesized by reducing a gold salt in an aqueous solution containing polymers. The gold@PVOH-b-PNVCL NPs exhibited temperature responsiveness and colloidal stability above their Lower Critical Solution Temperature (LCST). They were successfully loaded with Nadolol®, and the drug release was studied at different temperatures. PVOH-b-PNVCL copolymers with a slightly higher LCST than the biological temperature (37 °C) showed slower release at 37 °C but faster release at slightly higher temperatures. These results support the use of these thermo-responsive gold@PVOH-b-PNVCL NPs for drug delivery and controlled release. Furthermore, a study by Cao Yang et al. [9], explored the use of thermo-responsive Mn-Znferrite/poly(N,N'-isopropylacrylamide-co-N-hydroxymethylacrylamide core/shell nanocomposites for drug delivery systems. The thermo-responsive properties of the nanocomposites were studied, showing a significant response to temperature changes. Drug release tests revealed controlled release of the active ingredient, demonstrating the potential of these nanocomposites as drug delivery systems. These studies highlight the increasing importance of using thermo-sensitive core/shell NPs for controlled release of active ingredients. These systems offer advantages such as precise spatio-temporal control of release, improved bioavailability of active ingredients, and reduction of undesirable side effects [9]. Responsive nanocarrier were described recently by Mai et al., they have grown copolymer based on diethylene glycol methyl ether methacrylate, DEGMEMA, and oligoethylene glycol methyl ether methacrylate, OEGMEMA), from cubic iron oxide nanoparticle. The release of DOX was monitored after the heating of the NPs via alternating magnetic field (AMF) which induced a local heating of the NPs and the subsequent release of the DOX at the copolymer LCST. The authors have shown their smart nanosystem can display magnetic hyperthermia and a heat-mediated drug delivery properties by conducting in vitro and in vivo experiments [10]. Another interesting example from Coteh et al. Describe the grafting of a thermos-responsive polymer based on poly(ethyleneglycol methacrylate) on $CuFeS_2$ nanoparticles. The final nanomaterial has been shown to combine heat-mediated drug delivery and photothermal heat damage. The DOX release was obtained after the irradiation of the NPs by an NIR light which also led to a local heating of the NPs and the subsequent release of the drug [11]. Other nanomaterials structures were also investigated to lead to drug release of drug from inorganic core as organic metal framework (MOF) [12,13]. $Fe_{3-\delta}O_4$@UiO-66-NH$_2$, MOF were synthesized, the associated drug release behavior and anti-cancer activity were investigated showing an effective cytotoxicity when the nanomaterials were loaded by the anticancer drug [12]. These above presented examples are interesting, by the combination of at least two treatments against cancer cells, but the physical-chemical study of the drug release depending on the shell structure still lacks which is the purpose of this study. Thermo-responsive copolymers have indeed garnered significant interest in the field of drug delivery due to their ability to undergo phase transitions in response to temperature changes [14]. Among these copolymers, the combination of 2-(2-methoxy)

ethyl methacrylate (MEO$_2$MA) and oligo (ethylene glycol) methacrylate (OEGMA) has demonstrated remarkable thermo-responsive properties [15,16]. The preparation of thermo-sensitive copolymers based on MEO$_2$MA and OEGMA involves copolymerization of the two monomers [17]. This unique combination allows for the formation of copolymers that undergo a reversible hydrophilic-to-hydrophobic transition upon reaching the LCST [18]. The LCST of MEO$_2$MA/OEGMA copolymers can be tailored by adjusting the ratio of the two monomers [19]. Higher proportions of OEGMA result in a higher LCST, while higher proportions of MEO$_2$MA lead to a lower LCST [19]. This tunability allows the design of copolymers with LCSTs in the physiological temperature range, making them suitable for biomedical applications [20]. The preparation of MEO$_2$MA/OEGMA copolymers typically involves free radical polymerization techniques such as solution polymerization, emulsion polymerization, or reversible addition-fragmentation chain transfer (RAFT) polymerization [16]. These methods offer control over the copolymer composition and molecular weight, allowing for the customization of copolymer properties. The grafting of these MEO$_2$MA/OEGMA copolymers onto superparamagnetic iron oxide NPs provides a versatile platform for drug delivery, combining the advantages of the magnetic properties of the NPs and the thermo-responsive behavior of the copolymers [21]. This approach allows the precise control of drug release and can be used to specifically target areas of interest in the body, improving therapy efficacy and reducing undesirable side effects [22].

In this study, we developed core/shell NPs combining thermo-sensitive polymer brushes coated on a superparamagnetic iron oxide core for DOX loading and controlled release. The system consists of a Fe$_{3-\delta}$O$_4$ NPs core coated with a copolymer P(MEO$_2$MA$_x$-OEGMA$_{100-x}$) (where x and $100 - x$ represent the molar fractions of 2-(2-methoxy) ethyl methacrylate [MEO$_2$MA] and oligo (ethylene glycol) methacrylate [OEGMA], respectively) loaded with DOX, an anticancer drug. These NPs will be referred to as Fe$_{3-\delta}$O$_4$@P(MEO$_2$MA$_x$-OEGMA$_{100-x}$) NPs in this manuscript. The thermo-sensitive polymer was designed to have a LCST between 30 and 50 °C in PBS. The physicochemical characterizations of these Fe$_{3-\delta}$O$_4$@P(MEO$_2$MA$_x$-OEGMA$_{100-x}$) NPs have been published in previous reviews [22]. Here, we investigated the variation of the MEO$_2$MA and OEGMA monomer ratios to form copolymers on the surface of Fe$_{3-\delta}$O$_4$ NPs and their effects on both LCST and controlled release of DOX as a function of temperature and time. The results show the Fe$_{3-\delta}$O$_4$@P(MEO$_2$MA$_x$-OEGMA$_{100-x}$) NPs exhibited a DOX release profile dependent on their LCST, with sustained release over a period of 3 days. We believe these NPs hold promise for future use in cancer therapy. The results provide insight into the exciting developments of nanoparticle-based drug delivery systems for cancer treatment. By understanding the underlying principles of their preparation and potential applications, we can pave the way for the development of more effective and targeted therapeutic approaches, ultimately leading to better outcomes for cancer patients.

2. Materials and Methods

2.1. Materials

The synthesis of citrate-stabilized Fe$_{3-\delta}$O$_4$ magnetic NPs was carried out using ferric chloride hexahydrate (Lancaster, 98%), ferrous sulfate heptahydrate (Merck, 99.5%), ammonia (NH3, 28%), and sodium citrate (99.8%), purchased from Sigma–Aldrich. The polymerization initiators used were (chloromethyl) phenylethyl) trimethoxysilane (CMPETMS) (Gelest, >95%), tetramethylammonium hydroxide pentahydrate (TMAH) (99.8%), and toluene (laboratory reagent, >99.3%). For the surface-initiated polymerization of methacrylate, we used 2-(2-methoxy) ethyl P(MEO$_2$MAxOEGMA$_{100-x}$) (MEO$_2$MA) (98%), oligo (ethylene glycol) (OEGMA) (98%), N, N-dimethylformamide (DMF) (>99.8%), dimethyl sulfoxide (DMSO) (>99.8%), and Milli-Q water from Sigma–Aldrich.

2.2. Synthesis of Superparamagnetic Fe$_{3-\delta}$O$_4$ NPs

The synthesis of superparamagnetic Fe$_{3-\delta}$O$_4$ NPs (SPIONs) was carried out by co-precipitation [23]. A mixture of FeCl$_3\cdot$6H$_2$O (6 mmol; 1.622 g) and FeSO$_4\cdot$7H$_2$O (5 mmol;

1.39 g) was dissolved in forty mL of water in a three-neck flask. Then, 5 mL of a 28% (*v/v*) aqueous ammonia solution was added to the mixture, and the final solution was heated to 90 °C under magnetic stirring and an argon atmosphere. Subsequently, 4.4 g (14.9 mmol) of sodium citrate in 15 mL of water were added dropwise until a black solution was obtained. The reaction mixture was stirred for 30 min at 90 °C. The SPIONs were finally recovered by magnetic separation, washed several times with ethanol by centrifugation (14,000 rpm, 20 min), and redispersed in 100 mL of water.

2.3. Synthesis of CMPETMS-Coated $Fe_{3-\delta}O_4$ MNPs ($Fe_{3-\delta}O_4$@ Silane)

The SPIONs were dispersed in 10 mL of toluene under argon atmosphere. CMPETMS (0.2 mmol, 49.1 µL) was injected, and the mixture was stirred for 2 min. Then, 1 mL of an ethanolic solution of tetramethylammonium hydroxide pentahydrate (TMAOH) (36.25 mg) was added, and the mixture was stirred under argon for 15 min at 50 °C. The mixture was subsequently cooled to room temperature, and the SPIONs were separated by centrifugation. The silanized SPIONs were dispersed in 10 mL of toluene, and 2 mL of an ethanolic solution of TMAOH (36.25 mg) were injected. The reaction was carried out under argon for 30 min at 50 °C under magnetic stirring. The mixture was then cooled in a water bath, and the SPIONs were separated by centrifugation and washed twice with toluene.

2.4. Synthesis of $Fe_{3-\delta}O_4$@P($MEO_2MA_x-OEGMA_{100-x}$)

The growth of P(MEO_2MA_x-$OEGMA_{100-x}$) from the surface SPIONs was carried out using an adapted protocol described by Alem et al. [17]. In summary, in a 100 mL Schlenk flask, 50 mg of $Fe_{3-\delta}O_4$@silane MNP was dispersed in 10 mL of a DMF/DMSO mixture (10:90, *v/v*). Four samples containing different monomer percentages (MEOGA and OGMA) were added for the synthesis of $Fe_{3-\delta}O_4$@silane (Table 1). Once the MNPs were completely dispersed, 200 mL of a stored solution of $CuBr_2$/TPMA (0.884 mmol $CuBr_2$, 4.3 mmol TPMA) in DMSO were added to the mixture. The reaction mixture was stirred and heated at 65 °C. Then, 250 mL of a hydrazine mother solution in DMSO (7.1 mg mL^{-1}) was added, and the mixture was stirred for 2 h 65 °C under an argon atmosphere. At the end of the polymerization, the mixture was added dropwise to hot Milli-Q water to precipitate the insoluble components [24]. The materials were purified by redispersing the core/shell NPs in cold water, followed by centrifugation of the heated solution.

Table 1. Volumetric ratio of different prepared samples.

Samples	MEO$_2$MA	OEGMA
$Fe_{3-\delta}O_4$@P(MEO_2MA_{80}-$OEGMA_{20}$)	1.550 mL	0.571 mL
$Fe_{3-\delta}O_4$@P(MEO_2MA_{75}-$OEGMA_{25}$)	1.450 mL	0.714 mL
$Fe_{3-\delta}O_4$@P(MEO_2MA_{50}-$OEGMA_{50}$)	1 mL	1 mL
$Fe_{3-\delta}O_4$@P(MEO_2MA_{40}-$OEGMA_{60}$)	1.140 mL	1.160 mL

2.5. Drug Conjugation to MNCs

Conjugation of DOX with MNPs was accomplished by forming hydrogen bonds with the ether-oxide groups of the P(MEO_2MA-OEGMA) copolymer. DOX and MNCs were combined in DMEM (pH = 7.4) and gently agitated in the dark at room temperature for 24 h, facilitating the conjugation of DOX through the imine linkage. The resulting DOX-loaded MNCs (DOX-MNCs) were separated magnetically and thoroughly washed with DMEM until no DOX was detected in the supernatant (at least 10 washing cycles). The concentration of released DOX over time was determined by measuring the absorbance at 480 nm of the remaining free DOX in solution. The drug loading content (DLC), drug loading efficiency (DLE), and percentage of drug released (%) were then calculated using Equations (1)–(3).

$$\text{DLC(wt\%)} = \frac{\text{amount of DOX in the MNPs}}{\text{amount of MNPs}} \times 100\% \qquad (1)$$

$$\text{DLE(wt\%)} = \frac{\text{amount of DOX in the MNPs}}{\text{total amount of feeding drug}} \times 100\% \tag{2}$$

$$\text{percentage of drug released} = \frac{\text{mass of drug released}}{\text{mass of drug loaded}} \times 100\% \tag{3}$$

2.6. DOX Release Kinetics Analysis

To understand the drug release mechanism and rate, we applied several kinetic models to the obtained data. The models used for our system included the zero-order, first-order, Higuchi, and Korsmeyer–Peppas release models. By fitting the data to these models, we aimed to determine the most relevant model that described the drug release behavior [25,26].

The release kinetics of the zero-order model is influenced by the concentration of the drug and can be mathematically described as follows:

$$\mathbf{M_t = M_0 + k_0.t} \tag{4}$$

In this Equation (4), M_t represents the amount of drug dissolved at time t, M_0 represents the initial amount of drug in the solution (with $M_0 = 0$ in our case), and K_0 represents the zero-order release constant, which is expressed in units of concentration per time.

Moving on to the first-order kinetic release, it is also concentration-dependent and can be mathematically expressed as follows:

$$\mathbf{M_t = M_\infty[1 - exp(-k_1.t)]} \tag{5}$$

where M_0 is the initial concentration of a drug, K_1 is the first-order rate constant, and t is the time.

The Higuchi model is used to describe the release of a drug from solid matrices and is expressed as follows:

$$\mathbf{M_t = k_H.}t^{1/2} \tag{6}$$

where M_t represents the amount of drug released at time t, K_H is the Higuchi rate constant, and t is the time. The Higuchi model provides insights into the release behavior of drugs from solid matrices by relating the square root of time to the amount of drug released.

The Korsmeyer–Peppas model is a simplified relationship used to describe the release of a drug from a polymeric matrix. It is expressed as follows:

$$\mathbf{M_t/M_\infty = k_{kp} + t_n} \tag{7}$$

where M_t/M_∞ represents the fraction of drug released at time t, K_{Kp} is the Korsmeyer–Peppas release rate constant, n is the release exponent, and t is the time. This model allows for the characterization of the drug release mechanism and provides insights into the release kinetics from polymeric matrices.

3. Results

3.1. Colloidal Behavior of Nano-Objects in Physiological Environments

To study the influence of the environment and temperature on the colloidal properties of the copolymers in the $Fe_{3-\delta}O_4@P(MEO_2MA_X\text{-}OEGMA_{100-X})$ nanostructures, DLS analyses were performed on these nanostructures in an aqueous environment and in the physiological medium. The evolution of the hydrodynamic diameter of all samples for temperatures ranging from 25 to 50 °C is shown in Figure 1. Indeed, at low temperatures below the LCST, the MNPs do not exhibit any significant change in the average diameter. As the temperature increases, the average diameter of the MNPs abruptly increases to reach a stable value beyond which no significant further changes are observed [27].
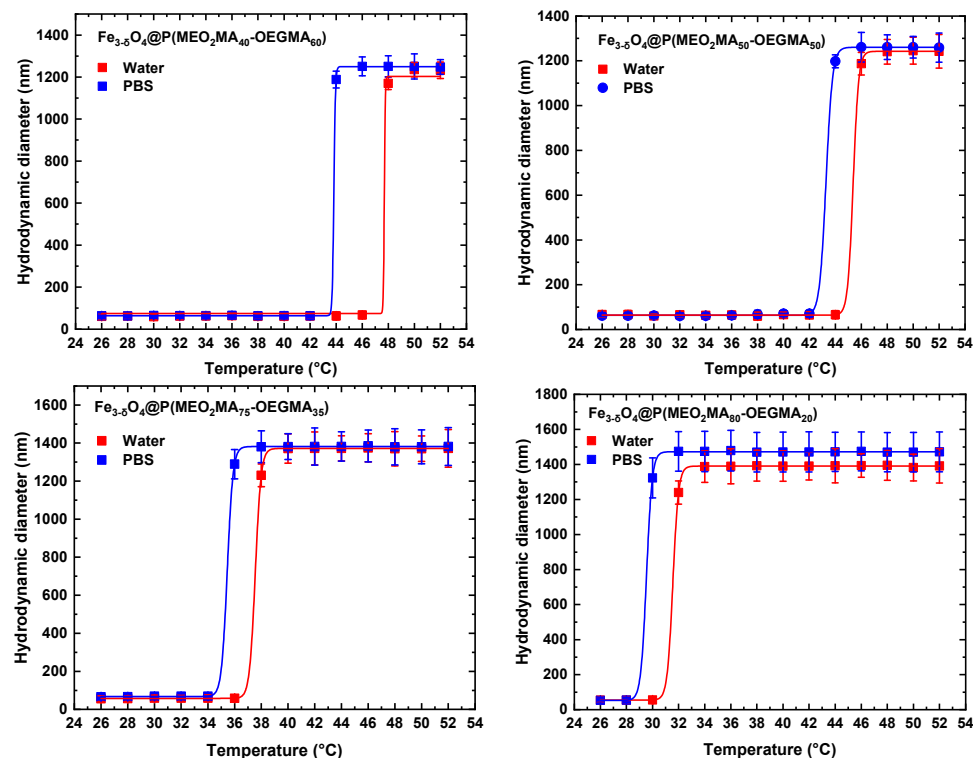
Figure 1. Evolution of the diameter of the $Fe_{3-\delta}O_4@P(MEO_2MA_X\text{-}OEGMA_{100-X})$ NPs with temperature in water and PBS.

Below the LCST, the hydrodynamic diameter was smaller because the core/shell MNPs have been dispersed in the aqueous medium owing to polymer chains being swollen by the solvent through hydrogen bonding between the polar groups of the copolymer and water [28,29]. Above the LCST, the organization of MNPs in the aqueous medium changes from dispersion to aggregation, as illustrated in Figure 1. This process occurs because when the temperature exceeds the LCST, the hydrogen bonds between water molecules are broken, causing polymer chains to precipitate onto the surface of the MNPs, making the surface hydrophobic [30]. This leads to the aggregation of MNPs in the aqueous medium and consequently the broadening of the peaks observed in DLS. The LCST values of $Fe_{3-\delta}O4@P(MEO_2MA_X\text{-}OEGMA_{100-X})$ NPs are shown in Table 2.

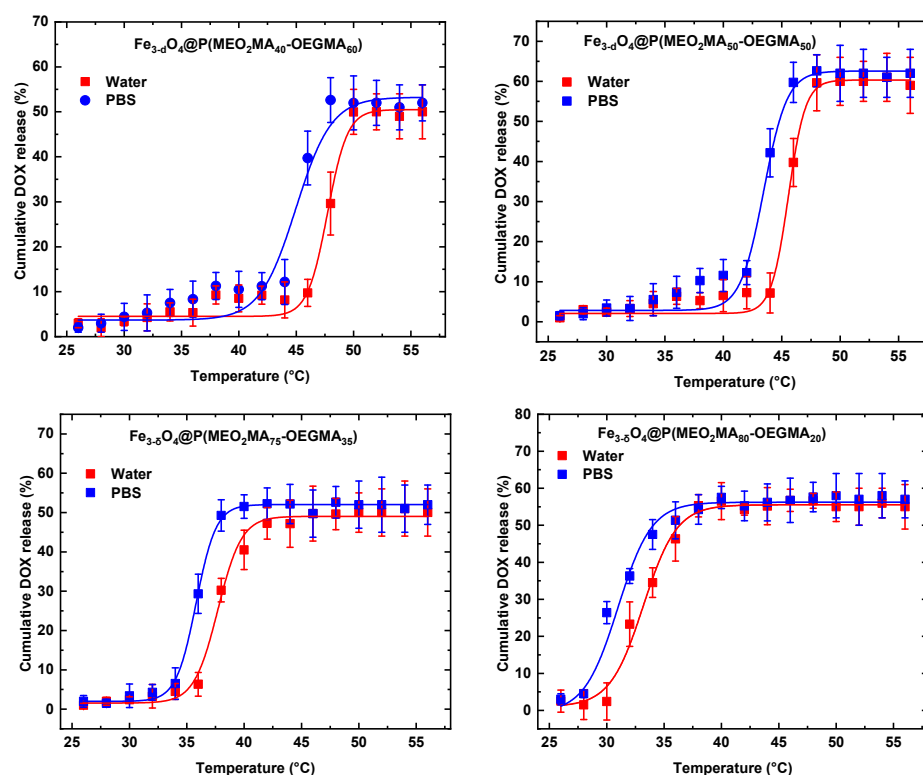**Table 2.** LCST values of $Fe_{3-\delta}O4@P(MEO_2MA_X\text{-}OEGMA_{100-X})$ NPs in water and in the PBS, determined by DLS.

Samples	LCST in Water (°C)	LCST in PBS (°C)
$Fe_{3-\delta}O_4@P(MEO_2MA_{80}\text{-}OEGMA_{20})$	32	30
$Fe_{3-\delta}O_4@P(MEO_2MA_{75}\text{-}OEGMA_{25})$	38	36
$Fe_{3-\delta}O_4@P(MEO_2MA_{50}\text{-}OEGMA_{50})$	45	43
$Fe_{3-\delta}O_4@P(MEO_2MA_{40}\text{-}OEGMA_{60})$	48	44

Furthermore, to investigate the reversibility (dispersion and aggregation) of our systems with temperature, we performed successive cycles of heating (T > LCST) and cooling (T < LCST). The results are presented in Figure S1, which shows the evolution of the hydrodynamic diameter as a function of temperature and confirms the processes are fully reversible. At 25 °C (below the LCST of $Fe_{3-\delta}O_4@P(MEO_2MA_X\text{-}OEGMA_{100-X})$ NPs), the hydrodynamic diameter is small as the NPs are well dispersed in the medium. However, at 50 °C (a temperature above the LCST of approximately 38 ± 7 °C for these MNPs), the hydrodynamic diameter increases due to MNPs aggregation.

3.2. Release of DOX as a Function of Temperature

The core/shell MNPs developed in this study were loaded with DOX in the copolymer chains through supramolecular interactions. Van der Waals dipole-dipole interactions can also be considered, but the main interactions that enable DOX penetration into these samples are hydrogen bonding interactions, as previously confirmed in our published works. Indeed, we favor supramolecular interactions to encapsulate DOX and develop a system that can rapidly release the drug with only a slight temperature increase. While the copolymer chains are swollen below the LCST due to hydrogen bonding with water molecules, DOX can diffuse into the copolymer shell and be blocked by hydrogen bonding interactions. Once the LCST is reached, the copolymer chains undergo a hydrophilic/hydrophobic transition and their collapse onto the surface of $Fe_{3-\delta}O_4$ NPs allows for the release of DOX. We chose to perform short-duration experiments (5 min) to demonstrate the effect of temperature on our core/shell MNPs. The cumulative release of DOX as a function of temperature for $Fe_{3-\delta}O_4@P(MEO_2MA_X-OEGMA_{100-X})$ NPs in water and PBS is depicted in Figure 2.


Figure 2. Cumulation curves of $Fe_{3-\delta}O_4@P(MEO_2MA_X-OEGMA_{100-X})$ NPs in water and PBS.

Surprisingly, there is almost negligible release of DOX for the four samples below the LCST (Figure 2). As the temperature increases, we observe a change in the slope of the curves as soon as the LCST is reached. Significant release occurs at 32, 38, 45, and 48 °C, respectively, for $Fe_{3-\delta}O_4@P(MEO_2MA_{80}-OEGMA_{20})$ NPs, $Fe_{3-\delta}O_4@P(MEO_2MA_{75}-OEGMA_{25})$ NPs, $Fe_{3-\delta}O_4@P(MEO_2MA_{50}-OEGMA_{50})$ NPs, and $Fe_{3-\delta}O_4@P(MEO_2MA_{40}-OEGMA_{60})$ NPs in water, and at 30, 36, 43, and 44 °C in PBS. These temperatures correspond to the LCST values of the samples in water and PBS, respectively.

3.3. Release Profile and Mechanism of DOX over Time

Based on the results from the first part, we selected two samples that exhibited an LCST higher than the physiological temperature (37 °C) to study the doxorubicin release kinetics at temperatures below and above the LCST in PBS. At a temperature lower than the LCST in PBS, the initial cumulative release proportion of DOX from

Fe$_{3-\delta}$O$_4$@P(MEO$_2$MA$_{40}$-OEGMA$_{60}$) NPs was approximately 18% up to 60 h (Figure 3). The DOX release rate from Fe$_{3-\delta}$O$_4$@P(MEO$_2$MA$_{50}$-OEGMA$_{50}$) NPs reached a maximum of 21% after 60 h at 37 °C. At a temperature above the LCST in PBS, a linear release of DOX was observed over time, reaching up to 100% after 60 h for both Fe$_{3-\delta}$O$_4$@P(MEO$_2$MA$_{40}$-OEGMA$_{60}$) NPs and Fe$_{3-\delta}$O$_4$@P(MEO$_2$MA$_{50}$-OEGMA$_{50}$) NPs (Figure 3). This linear DOX release behavior is induced by the hydrophilic/hydrophobic transition of P(MEO$_2$MA$_X$-OEGMA$_{100-X}$) observed after the LCST (Table 2). Additionally, initial releases of 21% and 24% were observed at 45 °C, respectively, for Fe$_{3-\delta}$O$_4$@P(MEO$_2$MA$_{40}$-OEGMA$_{60}$) NPs and Fe$_{3-\delta}$O$_4$@P(MEO$_2$MA$_{50}$-OEGMA$_{50}$) NPs. This can be explained by the fact that the chosen temperature was higher than the LCST of the copolymers.
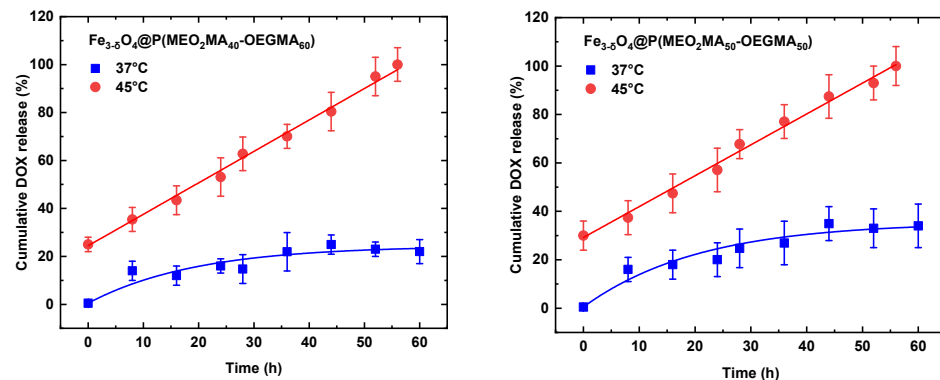
Figure 3. Release of DOX from Fe$_{3-\delta}$O$_4$@P(MEO$_2$MA$_X$-OEGMA$_{100-X}$) NPs in a PBS.

The parameters (K$_1$, K$_h$, K$_{kp}$, and n) of the previously described mathematical models for the release of DOX are presented in Table 3, along with the correlation values (R^2). The kinetic models of Higuchi and Korsmeyer–Peppas do not fit well with the experimental data, as indicated by the low R^2 values, while the first-order and zero-order kinetic models appear to be the most suitable for describing releases at temperatures below and above the LCST.

Table 3. Kinetics of DOX release from the Fe$_{3-\delta}$O$_4$@P(MEO$_2$MA$_X$-OEGMA$_{100-X}$) NPs.

Samples	T (°C)	Zero Order		First Order		Higushi		Korsmeyer-Peppas		
		K$_0$	R^2	K$_1$	R^2	K$_h$	R^2	K$_{kp}$	R^2	n
Fe$_{3-\delta}$O$_4$@P(MEO$_2$MA$_{40}$-OEGMA$_{60}$)	37	1.215	0.935	0.686	0.979	1.101	0.820	0.491	0.831	0.375
Fe$_{3-\delta}$O$_4$@P(MEO$_2$MA$_{50}$-OEGMA$_{50}$)	37	1.123	0.958	0.319	0.983	1.009	0.892	0.849	0.826	0.266
Fe$_{3-\delta}$O$_4$@P(MEO$_2$MA$_{40}$-OEGMA$_{60}$)	45	1.310	0.998	0.309	0.870	1.122	0.783	0.792	0.809	0.230
Fe$_{3-\delta}$O$_4$@P(MEO$_2$MA$_{50}$-OEGMA$_{50}$)	45	1.274	0.996	0.224	0.890	1.072	0.799	0.656	0.841	0.288

The equations associated with each of the MNPs are as follows:
for Fe$_{3-\delta}$O$_4$@P(MEO$_2$MA$_{40}$-OEGMA$_{60}$)-DOX at 45 °C:

$$C_{40/60}^{45°C}\ (\%) = 24.464 + 1.310\ t \tag{8}$$

for Fe$_{3-\delta}$O$_4$@P(MEO$_2$MA$_{50}$-OEGMA$_{50}$)-DOX at 45 °C:

$$C_{50/50}^{45°C}\ (\%) = 29.200 + 1.274\ t \tag{9}$$

for $Fe_{3-\delta}O_4@P(MEO_2MA_{40}\text{-}OEGMA_{60})\text{-}DOX$ at 37 °C:

$$C_{40/60}^{37°C}\ (\%) = 24.419 - 896.037/\left(1 + \exp\left(\frac{t + 68.706}{19.107}\right)\right) \tag{10}$$

for $Fe_{3-\delta}O_4@P(MEO_2MA_{50}\text{-}OEGMA_{50})\text{-}DOX$ at 37 °C:

$$C_{50/50}^{37°C}\ (\%) = 35.432 - 1203.334/\left(1 + \exp\left(\frac{t + 70.998}{20.226}\right)\right) \tag{11}$$

where $C_{y/z}^{x°C}$ (%) represents the percentage of cumulative DOX release, with x the temperature at which the kinetics were monitored, y the ratio of MEO_2MA, and z the ratio of OEGMA.

The DLC (%) and DLE (%) of the nano-systems reach 6.5% and 60% respectively for $Fe_{3-\delta}O_4@P(MEO_2MA_{40}\text{-}OEGMA_{60})$ NPs. We obtained similar values for the $Fe_{3-\delta}O_4@P(MEO_2MA_{50}\text{-}OEGMA_{50})$ NPs system, with a DLC of 6.2% and a DLE of 55% (all results were obtained from UV curves and data presented in Figure S2).

4. Discussion

Copolymer-based NPs offer numerous advantages as drug delivery systems [31]. They can be designed to enhance drug solubility, prolong its half-life in the body, and specifically target cancer cells [32]. In this study, the copolymer used was composed of MEO_2MA and OEGMA. These two monomers impart specific properties to the final copolymer [22]. The composition of the copolymer can influence both the LCST and the drug loading capacity and release rate of doxorubicin [19]. Indeed, the results of the evolution of the hydrodynamic diameter of $Fe_{3-\delta}O_4@P(MEO_2MA_X\text{-}OEGMA_{100-X})$ NPs as a function of temperature confirm the influence of the number of ether-oxide groups on the LCST value. Previous studies have shown as the number of ether-oxide groups in the monomer units of the copolymers increased, the LCST was shifted towards higher temperatures [22,33]. For instance, studies conducted by Qian Li et al. [34] and Yanfei Hua et al. [35] examined MEO_2MA and OEGMA copolymers and demonstrated the LCST increased with an increase in the OEGMA content in the copolymer. Specifically, they observed copolymers containing a higher amount of OEGMA exhibited a higher LCST compared to those with a lower amount of OEGMA. We have shown increasing the amounts of OEGMA in the samples led to a shift in the LCST towards higher temperatures, all the results were gathered in Table 2. For example, the sample containing 20% OEGMA exhibits an LCST of 33 °C in water, while the sample with 60% OEGMA reaches an LCST of 48 °C. This confirms increasing the number of ether-oxide groups results in an increase in the temperature at which the copolymers undergo separation and aggregation. Additionally, the $Fe_{3-\delta}O_4@P(MEO_2MA_X\text{-}OEGMA_{100-X})$ NPs demonstrate a significant change in LCST in water and PBS, leading to notable aggregation. This indicates these MNPs are temperature-sensitive and can undergo a transition of separation and aggregation depending on the environmental conditions [19]. Furthermore, kosmotropic anions have a polarizing effect that weakens the hydrogen bonding between water molecules and ether groups present in the $P(MEO_2MA_X\text{-}OEGMA_{100-X})$ copolymers [25,36]. As a consequence, this leads to a decrease in the LCST in physiological environments [25]. Furthermore, we demonstrated at a temperature below the LCST for $Fe_{3-\delta}O_4@P(MEO_2MA_X\text{-}OEGMA_{100-X})$ NPs, the hydrodynamic diameter was small because the NPs were well dispersed in the medium. This means the MNPs remain in their individual form and do not aggregate at this temperature. This is due to the interaction between the ether-oxide groups present in the copolymer and the surrounding medium, which keeps the NPs dispersed. However, at a temperature of 50 °C (above the LCST), the hydrodynamic diameter increases due to nanoparticle aggregation. At this temperature, the copolymer undergoes a phase transition and becomes insoluble in the medium, leading to nanoparticle aggregation. The interaction between the ether-oxide groups is disrupted, and the NPs cluster together to form larger aggregates. When the temperature is lowered

again, the copolymer rehydrates and regains its nanoparticle dispersing capability. During the cooling process, the ether-oxide groups re-establish their interaction with the surrounding medium, allowing for nanoparticle dispersion. This behavior is consistent with the high hydration capacity of ethylene glycol and the groups present in the $P(MEO_2MA_X\text{-}OEGMA_{100-X})$ copolymer at temperatures below the LCST. The composition of copolymers based on MEO2MA and OEGMA has a significant impact on the control of DOX release. For instance, NPs $Fe_{3-\delta}O_4@P(MEO_2MA_{40}\text{-}OEGMA_{60})$ NPs and $_{Fe3-\delta}O_4@P(MEO_2MA_{50}\text{-}OEGMA_{50})$ NPs, which contain a higher amount of OEGMA, exhibit a narrower temperature range between the beginning of drug release and complete release compared to NPs with a lower amount of OEGMA ($Fe_{3-\delta}O_4@P(MEO_2MA_{75}\text{-}OEGMA_{25})$ NPs and $Fe_{3-\delta}O_4@P(MEO_2MA_{80}\text{-}OEGMA_{20})$ NPs). However, only approximately $55 \pm 3\%$ and $57 \pm 4\%$ of the total amount of DOX were released within a very short time period of about 10 min for $Fe_{3-\delta}O_4@P(MEO_2MA_{40}\text{-}OEGMA_{60})$ NPs and $Fe_{3-\delta}O_4@P(MEO_2MA_{50}\text{-}OEGMA_{50})$ NPs, and around $50 \pm 4\%$ and $52 \pm 5\%$ for $Fe_{3-\delta}O_4@P(MEO2MA_{75}\text{-}OEGMA_{25})$ NPs and $Fe_{3-\delta}O_4@P(MEO_2MA_{80}\text{-}OEGMA_{20})$ NPs, respectively. These results indicate rapid diffusion of DOX out of the copolymer with a higher amount of OEGMA but also the need for a longer duration to achieve complete release of the active compound. Furthermore, the release kinetics of $Fe_{3-\delta}O_4@P(MEO_2MA_{40}\text{-}OEGMA_{60})$ NPs and $Fe_{3-\delta}O_4@P(MEO_2MA_{50}\text{-}OEGMA_{50})$ NPs demonstrated a linear release profile at a temperature of approximately 45 °C (above the LCST of both samples), with a significant difference in the slope. Specifically, the slope was approximately 1.311 for $Fe_{3-\delta}O_4@P(MEO_2MA_{40}\text{-}OEGMA_{60})$ NPs and 1.211 for $Fe_{3-\delta}O_4@P(MEO_2MA_{50}\text{-}OEGMA_{50})$ NPs, indicating a slower release for the sample with 60% MEO_2MA compared to the sample with 50% MEO_2MA. Additionally, the influence of copolymer composition was also observed in the values of DLC and DLE, where significant differences were observed between the two samples with 60% MEO_2MA and the sample with 50% MEO_2MA. Furthermore, for the $Fe_{3-\delta}O_4@P(MEO_2MA_{40}\text{-}OEGMA_{60})$ NPs, we obtain a DLC of 6.5%, indicating 6.5% of the total mass of the NPs consists of DOX. This suggests the NPs can load a significant amount of DOX. Additionally, the DLE reaches 60%, meaning 60% of the DOX present in the system is efficiently encapsulated within the NPs. This demonstrates a good encapsulation capacity of DOX by the $Fe_{3-\delta}O_4@P(MEO_2MA_{40}\text{-}OEGMA_{60})$ NPs copolymer, which is essential for ensuring controlled release and optimal therapeutic efficacy. For the $Fe_{3-\delta}O_4@P(MEO_2MA_{50}\text{-}OEGMA_{50})$ NPs, the DLC and DLE values are slightly lower. The DLC is equal to 6.2%, indicating the amount of DOX loaded into the NPs is slightly reduced compared to the previous sample. The DLE is equal to 55%, meaning 55% of the DOX is efficiently encapsulated within the NPs. Although slightly lower, these values remain significant and indicate a substantial loading and encapsulation capacity for the $Fe_{3-\delta}O_4@P(MEO_2MA_{50}\text{-}OEGMA_{50})$ NPs. Comparing the two samples, we observe the composition of the copolymer based on MEO_2MA and OEGMA slightly influences the DLC and DLE values. The $Fe_{3-\delta}O_4@P(MEO_2MA_{40}\text{-}OEGMA_{60})$ NPs exhibit a slightly higher DLC, suggesting a slightly higher loading capacity for DOX compared to the $Fe_{3-\delta}O_4@P(MEO_2MA_{50}\text{-}OEGMA_{50})$ NPs system. Similarly, the DLE is also slightly higher for the $Fe_{3-\delta}O_4@P(MEO_2MA_{40}\text{-}OEGMA_{60})$ NPs, indicating a better encapsulation efficiency of DOX. However, both systems show significant DLC and DLE values, confirming their ability to effectively load and encapsulate DOX. The DLC value is close to those reported in the literature for nano-objects with a similar structure [29,37,38]. The DLC (%) and DLE (%) values for our MNPs and some vectors from the literature are presented in Table 4. A study by Nidhi Andhariya et al. [39] explored a thermo-sensitive core/shell NPs composed of iron oxide NPs (Fe_3O_4) and a polymer (polyethylene oxide—poly D, L lactide-co-glycolide—polyethylene oxide (PEO-PLGA-PEO)). These nano-objects showed DLC values around 8.1% and a DLE value of approximately 89% [39]. The teams of Binh T Mai et al. [10] and Aziliz Hervault et al. [36] demonstrated with the same core/shell structure, they obtained DLC and DLE values around our values (Table 4).

Table 4. Comparison of DLC and DLE values of the nano-objects described in this work and other described in the literature.

Samples	DLC (%)	DLE (%)
$Fe_{3-\delta}O_4@P(MEO_2MA_{40}\text{-}OEGMA_{60})$	6.5	60
$Fe_{3-\delta}O_4@P(MEO_2MA_{50}\text{-}OEGMA_{50})$	6.2	55
$Fe_{3-\delta}O_4@P(DEGMA\text{-}co\text{-}PEGMA\text{-}b\text{-}[TMSPMA\text{-}co\text{-}VBA])$	7.6 [26]	82.3 [26]
$Fe_{3-\delta}O_4@P(DEGMEA\text{-}co\text{-}OEGMEMA)$	3.29 [29]	---
$Fe_3O_4@PEO\text{-}PLGA\text{-}PEO$	7.2 [28]	23.1 [28]
DOX-MNPs	8.1 [31]	90 [31]
DOX-AF-PNIPAM-Fe_3O_4	23 [32]	74.4 [32]

In summary, the composition of copolymers based on MEO_2MA and OEGMA plays a crucial role in controlling the release of DOX. A higher amount of OEGMA can influence the temperature range of release, release kinetics, as well as the loading and efficiency parameters of DOX release. These findings underscore the importance of optimizing copolymer composition to achieve controlled release.

5. Conclusions

The core/shell NPs $Fe_{3-\delta}O_4@P(MEO_2MA_X\text{-}OEGMA_{100-X})$ were synthesized using the ATRP SI-ARGET method, where the $P(MEO_2MA_x\text{-}OEGMA_{100-x})$ copolymers were grown on the surface. These core/shell NPs exhibit a thermo-sensitive behavior that can be controlled by adjusting the molar ratio of the MEO_2MA and OEGMA monomers. Their thermal response, characterized by the LCST, showed lower values in PBS compared to water. In vitro studies on the release of DOX from these core/shell NPs revealed the control and release rate strongly depended on the molar ratio used to form the copolymers. We demonstrated a higher amount of MEO_2MA could result in prolonged release as well as higher values of DLC and DLE. These findings provide a promising pathway for the design of novel therapeutic tools against cancer.

Supplementary Materials: The following supporting information can be downloaded at: https://www.mdpi.com/article/10.3390/colloids8010001/s1, Figure S1: Reversibility of the hydrodynamic diameter evolution with successive heating and cooling cycles in PBS of (a) $Fe_{3-\delta}O4@P(MEO_2MA_{40}\text{-}OEGMA_{60})$ NPs, (b) $Fe_{3-\delta}O4@P(MEO_2MA_{50}\text{-}OEGMA_{50})$ NPs, (c) $Fe_{3-\delta}O4@P(MEO_2MA_{75}\text{-}OEGMA_{25})$ NPs and (d) $Fe_{3-\delta}O4@P(MEO_2MA_{80}\text{-}OEGMA_{20})$ NPs.; Figure S2: Absorbances of different DOX concentration solutions (a) and Calibration curve of DOX (b).

Author Contributions: Conceptualization, H.A., E.G. and Z.F. methodology, Z.F. and H.A.; software, Z.F.; validation H.A., E.G. and Z.F.; formal analysis, Z.F.; investigation, Z.F.; resources H.A.; data curation, Z.F.; writing—original draft preparation, Z.F.; writing—review and editing, H.A., E.G. and Z.F.; visualization, H.A., E.G. and Z.F.; supervision, H.A., E.G.; project administration, H.A.; funding acquisition, H.A. and E.G. All authors have read and agreed to the published version of the manuscript.

Data Availability Statement: The data can be available on demand to the authors.

Conflicts of Interest: The authors declare no conflict of interest.

References

1. Debela, D.T.; Muzazu, S.G.Y.; Heraro, K.D.; Ndalama, M.T.; Mesele, B.W.; Haile, D.C.; Kitui, S.K.; Manyazewal, T. New approaches and procedures for cancer treatment: Current perspectives. *SAGE Open Med.* **2021**, *9*, 205031212110343. [CrossRef] [PubMed]
2. Ma, X.; Yu, H. Global burden of cancer. *Yale J. Biol. Med.* **2006**, *79*, 85–94. [PubMed]
3. Bachelard, C.M.; Coquan, E.; Rusquec, P.D.; Paoletti, X.; Tourneau, C.L. Risks and benefits of anticancer drugs in advanced cancer patients: A systematic review and meta-analysis. *eClinicalMedicine* **2021**, *40*, 101130. [CrossRef] [PubMed]
4. Rallis, K.S.; Yau, T.H.L.; Sideris, M. Chemoradiotherapy in Cancer Treatment: Rationale and Clinical Applications. *Anticancer Res.* **2021**, *41*, 1–7. [CrossRef] [PubMed]

5. Szczęch, M.; Szczepanowicz, K. Polymeric Core-Shell Nanoparticles Prepared by Spontaneous Emulsification Solvent Evaporation and Functionalized by the Layer-by-Layer Method. *Nanomaterials* **2020**, *10*, 496. [CrossRef] [PubMed]

6. Menon, J.U.; Kuriakose, A.; Iyer, R.; Hernandez, E.; Gandee, L.; Zhang, S.; Takahashi, M.; Zhang, Z.; Saha, D.; Nguyen, K.T. Dual-Drug Containing Core-Shell Nanoparticles for Lung Cancer Therapy. *Sci. Rep.* **2017**, *7*, 13249. [CrossRef] [PubMed]

7. Deshpande, S.; Sharma, S.; Koul, V.; Singh, N. Core–Shell Nanoparticles as an Efficient, Sustained, and Triggered Drug-Delivery System. *ACS Omega* **2017**, *2*, 6455–6463. [CrossRef]

8. Liu, J.; Detrembleur, C.; Hurtgen, M.; Debuigne, A.; De Pauw-Gillet, M.-C.; Mornet, S.; Duguet, E.; Jérôme, C. Thermo-responsive gold/poly(vinyl alcohol)-b-poly(N-vinylcaprolactam) core–corona nanoparticles as a drug delivery system. *Polym. Chem.* **2014**, *5*, 5289–5299. [CrossRef]

9. Yang, C.; Jie, R.; Jianbo, L.; Yan, L. Thermo-Responsive Mn–Zn Ferrite/Poly(N,N′-Isopropyl Acrylamide-co-N-Hydroxymethylacrylamide) Core/Shell Nanocomposites for Drug-Delivery Systems. *J. Biomater. Sci. Polym. Ed.* **2011**, *22*, 1473–1486. [CrossRef]

10. Mai, B.T.; Balakrishnan, P.B.; Barthel, M.J.; Piccardi, F.; Niculaes, D.; Marinaro, F.; Fernandes, S.; Curcio, A.; Kakwere, H.; Autret, G.; et al. Thermo-Responsive Iron Oxide Nanocubes for an Effective Clinical Translation of Magnetic Hyperthermia and Heat-Mediated Chemotherapy. *ACS Appl. Mater. Interfaces* **2019**, *11*, 5727–5739. [CrossRef]

11. Conteh, J.S.; Nucci, G.E.P.; Cabada, T.F.; Mai, B.T.; Soni, N.; De Donato, F.; Pasquale, L.; Catalano, F.; Prato, M.; Manna, L.; et al. CuFeS2 Nanoparticles Functionalized with a Thermoresponsive Polymer for Photothermia and Externally Controlled Drug Delivery. *ACS Appl. Mater. Interfaces* **2023**, *15*, 22999–23011. [CrossRef] [PubMed]

12. Shahin, R.; Yousefi, M.; Ziyadi, H.; Bikhof, M.; Hekmati, M. pH-Responsive and magnetic Fe3O4@UiO-66-NH2@PEI nanocomposite as drug nanocarrier: Loading and release study of Imatinib. *Inorg. Chem. Commun.* **2023**, *147*, 110186. [CrossRef]

13. Abdollahy, M.; Peyman, H.; Roshanfekr, H.; Idris, A.O.; Azizi, S.; Sibali, L.L. Synthesis and characterization of a smart polymer-coated core–shell MnFe2O4@ organometallic framework for targeted drug delivery. *Chem. Pap.* **2023**, *77*, 3897–3909. [CrossRef]

14. Gandhi, A.; Paul, A.; Sen, S.O.; Sen, K.K. Studies on thermoresponsive polymers: Phase behaviour, drug delivery and biomedical applications. *Asian J. Pharm. Sci.* **2015**, *10*, 99–107. [CrossRef]

15. Lutz, J.-F.; Weichenhan, K.; Akdemir, Ö.; Hoth, A. About the Phase Transitions in Aqueous Solutions of Thermoresponsive Copolymers and Hydrogels Based on 2-(2-methoxyethoxy)ethyl Methacrylate and Oligo(ethylene glycol) Methacrylate. *Macromolecules* **2007**, *40*, 2503–2508. [CrossRef]

16. Lapresta-Fernández, A.; Salinas-Castillo, A.; Capitán-Vallvey, L.F. Synthesis of a thermoresponsive crosslinked MEO2MA polymer coating on microclusters of iron oxide nanoparticles. *Sci. Rep.* **2021**, *11*, 3947. [CrossRef] [PubMed]

17. Alem, H.; Schejn, A.; Roques-Carmes, T.; Ghanbaja, J.; Schneider, R. Thermo-responsive and aqueous dispersible ZnO/PNIPAM core/shell nanoparticles. *Nanotechnology* **2015**, *26*, 335605. [CrossRef]

18. Alejo, T.; Prieto, M.; García-Juan, H.; Andreu, V.; Mendoza, G.; Sebastián, V.; Arruebo, M. A facile method for the controlled polymerization of biocompatible and thermoresponsive oligo(ethylene glycol) methyl ether methacrylate copolymers. *Polym. J.* **2018**, *50*, 203–211. [CrossRef]

19. Al Dine, E.J.; Ferjaoui, Z.; Ghanbaja, J.; Roques-Carmes, T.; Meftah, A.; Hamieh, T.; Toufaily, J.; Schneider, R.; Marchal, S.; Gaffet, E.; et al. Thermo-responsive magnetic Fe 3 O 4 @P(MEO 2 MA X -OEGMA 100-X) NPs and their applications as drug delivery systems. *Int. J. Pharm.* **2017**, *532*, 738–747. [CrossRef]

20. Xu, J.; Abetz, V. Nonionic UCST–LCST Diblock Copolymers with Tunable Thermoresponsiveness Synthesized via PhotoRAFT Polymerization. *Macromol. Rapid Commun.* **2021**, *42*, 2000648. [CrossRef]

21. Gambinossi, F.; Chanana, M.; Mylon, S.E.; Ferri, J.K. Programming nanoparticle aggregation kinetics with poly(MeO2MA-co-OEGMA) copolymers. *Soft Matter* **2013**, *9*, 11046. [CrossRef]

22. Ferjaoui, Z.; Schneider, R.; Meftah, A.; Gaffet, E.; Alem, H. Functional responsive superparamagnetic core/shell nanoparticles and their drug release properties. *RSC Adv.* **2017**, *7*, 26243–26249. [CrossRef]

23. Ferjaoui, Z.; Nahle, S.; Chang, C.S.; Ghanbaja, J.; Joubert, O.; Schneider, R.; Ferrari, L.; Gaffet, E.; Alem, H. Layer-by-Layer Self-Assembly of Polyelectrolytes on Superparamagnetic Nanoparticle Surfaces. *ACS Omega* **2020**, *5*, 4770–4777. [CrossRef] [PubMed]

24. Jańczewski, D.; Tomczak, N.; Han, M.-Y.; Vancso, G.J. Introduction of Quantum Dots into PNIPAM microspheres by precipitation polymerization above LCST. *Eur. Polym. J* **2009**, *45*, 1912–1917. [CrossRef]

25. Ferjaoui, Z.; Al Dine, E.J.; Kulmukhamedova, A.; Bezdetnaya, L.; Chang, C.S.; Schneider, R.; Mutelet, F.; Mertz, D.; Begin-Colin, S.; Quilès, F.; et al. Doxorubicin-Loaded Thermoresponsive Superparamagnetic Nanocarriers for Controlled Drug Delivery and Magnetic Hyperthermia Applications. *ACS Appl. Mater. Interfaces* **2019**, *11*, 30610–30620. [CrossRef] [PubMed]

26. Ferjaoui, Z.; Nahle, S.; Schneider, R.; Kerdjoudj, H.; Mertz, D.; Quilès, F.; Ferji, K.; Gaffet, E.; Alem, H. Development of Folate-Superparamagnetic Nanoconjugates for Inhibition of Cancer Cell Proliferation. *Adv. Mater. Interfaces* **2023**, *10*, 2202364. [CrossRef]

27. Miclotte, M.P.J.; Varlas, S.; Reynolds, C.D.; Rashid, B.; Chapman, E.; O'Reilly, R.K. Thermoresponsive Block Copolymer Core–Shell Nanoparticles with Tunable Flow Behavior in Porous Media. *ACS Appl. Mater. Interfaces* **2022**, *14*, 54182–54193. [CrossRef]

28. Murdoch, T.J.; Humphreys, B.A.; Johnson, E.C.; Prescott, S.W.; Nelson, A.; Wanless, E.J.; Webber, G.B. The role of copolymer composition on the specific ion and thermo-response of ethylene glycol-based brushes. *Polymer* **2018**, *138*, 229–241. [CrossRef]

29. Dalgakiran, E.; Tatlipinar, H. The role of hydrophobic hydration in the LCST behaviour of POEGMA300 by all-atom molecular dynamics simulations. *Phys. Chem. Chem. Phys.* **2018**, *20*, 15389–15399. [CrossRef]

30. Teotia, A.K.; Sami, H.; Kumar, A. Thermo-Responsive Polymers: Structure and Design of Smart Materials. In *Switchable and Responsive Surfaces and Materials for Biomedical Applications*; Zhang, Z., Ed.; Woodhead Publishing: Oxford, UK, 2015; pp. 3–43. [CrossRef]

31. Wang, Y.; Gao, S.; Ye, W.-H.; Yoon, H.S.; Yang, Y.-Y. Co-delivery of drugs and DNA from cationic core–shell nanoparticles self-assembled from a biodegradable copolymer. *Nat. Mater.* **2006**, *5*, 791–796. [CrossRef]

32. Yao, Y.; Zhou, Y.; Liu, L.; Xu, Y.; Chen, Q.; Wang, Y.; Wu, S.; Deng, Y.; Zhang, J.; Shao, A. Nanoparticle-Based Drug Delivery in Cancer Therapy and Its Role in Overcoming Drug Resistance. *Front. Mol. Biosci.* **2020**, *7*, 193. [CrossRef] [PubMed]

33. da Silva, M.A.; Haddow, P.; Kirton, S.B.; McAuley, W.J.; Porcar, L.; Dreiss, C.A.; Cook, M.T. Thermoresponsive Triblock-Copolymers of Polyethylene Oxide and Polymethacrylates: Linking Chemistry, Nanoscale Morphology, and Rheological Properties. *Adv. Funct. Mater.* **2022**, *32*, 2109010. [CrossRef]

34. Li, Q.; Wang, L.; Chen, F.; Constantinou, A.P.; Georgiou, T.K. Thermoresponsive oligo(ethylene glycol) methyl ether methacrylate based copolymers: Composition and comonomer effect. *Polym. Chem.* **2022**, *13*, 2506–2518. [CrossRef]

35. Hu, Y.; Darcos, V.; Monge, S.; Li, S. Thermo-responsive drug release from self-assembled micelles of brush-like PLA/PEG analogues block copolymers. *Int. J. Pharm.* **2015**, *491*, 152–161. [CrossRef]

36. Hervault, A.; Dunn, A.E.; Lim, M.; Boyer, C.; Mott, D.; Maenosono, S.; Thanh, N.T.K. Doxorubicin loaded dual pH- and thermo-responsive magnetic nanocarrier for combined magnetic hyperthermia and targeted controlled drug delivery applications. *Nanoscale* **2016**, *8*, 12152–12161. [CrossRef] [PubMed]

37. Shen, S.; Wu, Y.; Liu, Y.; Wu, D. High drug-loading nanomedicines: Progress, current status, and prospects. *Int. J. Nanomed.* **2017**, *12*, 4085–4109. [CrossRef]

38. Mura, S.; Nicolas, J.; Couvreur, P. Stimuli-responsive nanocarriers for drug delivery. *Nat. Mater.* **2013**, *12*, 991–1003. [CrossRef]

39. Andhariya, N.; Chudasama, B.; Mehta, R.V.; Upadhyay, R.V. Biodegradable thermoresponsive polymeric magnetic nanoparticles: A new drug delivery platform for doxorubicin. *J. Nanopart. Res.* **2011**, *13*, 1677–1688. [CrossRef]